

Limiters startup experiments in WEST on bulk tungsten tiles

P. Manas¹, R. A. Pitts², J. Hobirk³, P. Maget¹, A. Gallo¹, E. Geulin¹, A. Grosjean⁴ J. Gunn¹, C. Guillemaut¹, B. Guillermin¹, R. Mitteau¹, G. Ciraolo¹, N. Fedorczak¹, N. Varadarajan¹, the EUROfusion WPTE team* and the WEST Team**

¹ CEA, IRFM, F-13108 Saint-Paul-lez-Durance, France

² ITER Organization, Route de Vinon-sur-Verdon, 13067 St. Paul-lez-Durance Cedex, France

³ Max-Planck-Institut für Plasmaphysik, Boltzmannstr. 2, 85748 Garching, Germany

⁴ Department of Nuclear Engineering, University of Tennessee, Knoxville, Tennessee 37996, USA

* see the author list of E. Joffrin et al 2024 Nucl. Fusion 64 112019

** see <http://west.cea.fr/WESTteam>

Understanding and optimizing the startup phase in limiter configuration on tungsten components is critical for tokamak operation. This renewed interest in accurately modelling such phases has also been partly triggered by the rebaselining of ITER after the elimination of beryllium (Be) in favour of tungsten (W) [1,11]. While high performance ITER phases are less critical in terms of tungsten accumulation, the current ramp-up in a limiter configuration could result in such accumulation or radiative collapses, [11,2]. For current tokamak operation this phase is also important to optimize as was shown during the WEST campaigns prior to 2020 where the 6 inner limiters were equipped with W coated tiles resulting in difficult operation with cold and MHD prone plasmas [3]. This was one of the reasons to move to low Z material between 2020 and early 2024 with BN tiles [4] before transitioning to full W tiles end of 2024. In this context this transition was leveraged to provide quantitative analysis on restart conditions in BN vs W tiles. Finally, several actuators can be used to optimize this limiter phase, either transiently with boronisations, including central heating with ECRH [5] to minimize the cooling impact of tungsten, or using nitrogen seeding [6].

First, the startup on the newly installed W inner limiter tiles on the high field side have been attempted without boronisation. This followed a machine opening and standard conditioning (baking at ~190°C and glow discharge). Plasmas up to 1.5 s and 600 kA were obtained featuring significant outgassing and uncontrolled density trajectories. Most plasmas were cold and dense with radiated power fractions >70%. Visible spectroscopy shows dominant presence of oxygen, carbon, nitrogen but no sign of tungsten sources on the inner limiter (Fig. 1). Langmuir probes on one inner limiter provided data (Tantalum probes embedded in the tungsten tiles in the lower half of the limiter) with electron temperatures below 10 eV. After several attempts at trying to achieve stable flattops in limiter configuration, and without signs of core W contamination yet, it was decided to boronise. Similar issues were also encountered during a restart with low Z material (Fig. 2).

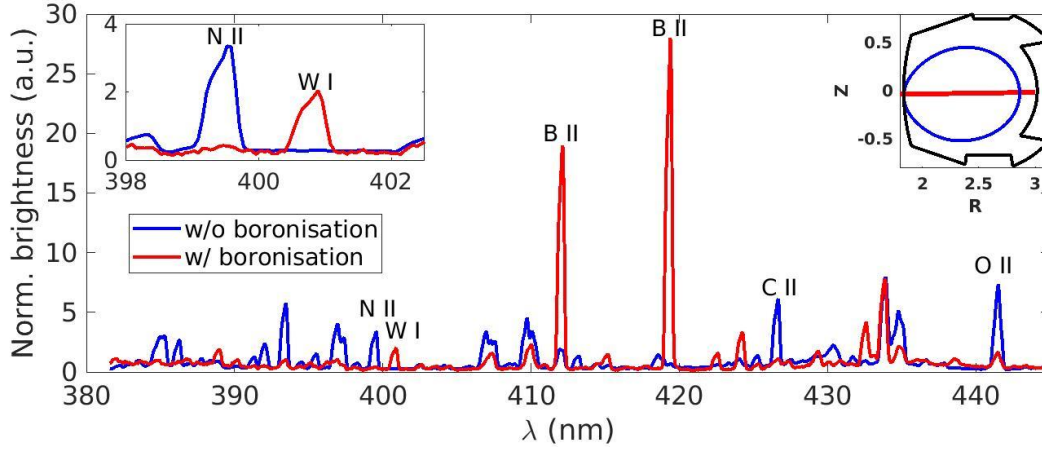


Figure 1: Time averaged, normalized brightness visible spectra from the central line of sight looking at one inner tungsten limiter. Data prior and following a non-uniform boronisation are shown.

First ohmic plasmas of 10 s in limiter configuration were obtained directly following a non-uniform boronisation (half injection points). The first two pulses were obtained with very low densities ($\bar{n} \approx 0.5 \times 10^{19} \text{ m}^{-3}$) at 300 kA and steady increase of the tungsten visible line intensity was observed. Three consecutive

ohmic shots were also performed to characterize the impact of the distance to boronisation on the W source and plasma performances. Fuelling and density trajectories are found different (impact of boronisation on D_2 retention fading away) and the central electron temperature is decreasing from shot to shot (flatter core profiles) with clear signs of increased central radiation (Fig. 3). The impact of increased W core contamination/transport on core parameters is further investigated in the following with core integrated modelling.

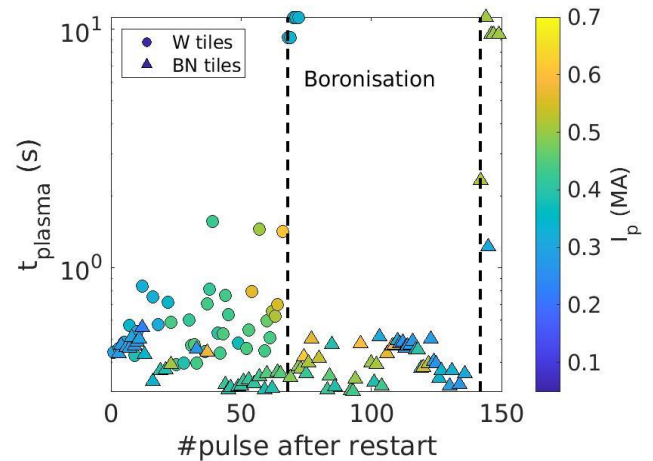


Figure 2: Plasma duration for ohmic plasmas directly following an experimental campaign restart with inner limiters equipped with either BN or W tiles.

Scans in plasma densities and currents were also performed to provide a range of relevant data to be analysed and modelled with Greenwald fractions ranging from ~15% to ~90% and plasma current from 300 to 700 kA. At these higher I_p , strong outgassing was observed together with high apparent temperatures found above 600°C on lateral tiles with the wide angle infrared camera. Finally several pulses have been performed further away from the boronisation during this experimental campaign showing the limited access to low densities as expected and the

presence of runaways far from boronisation.

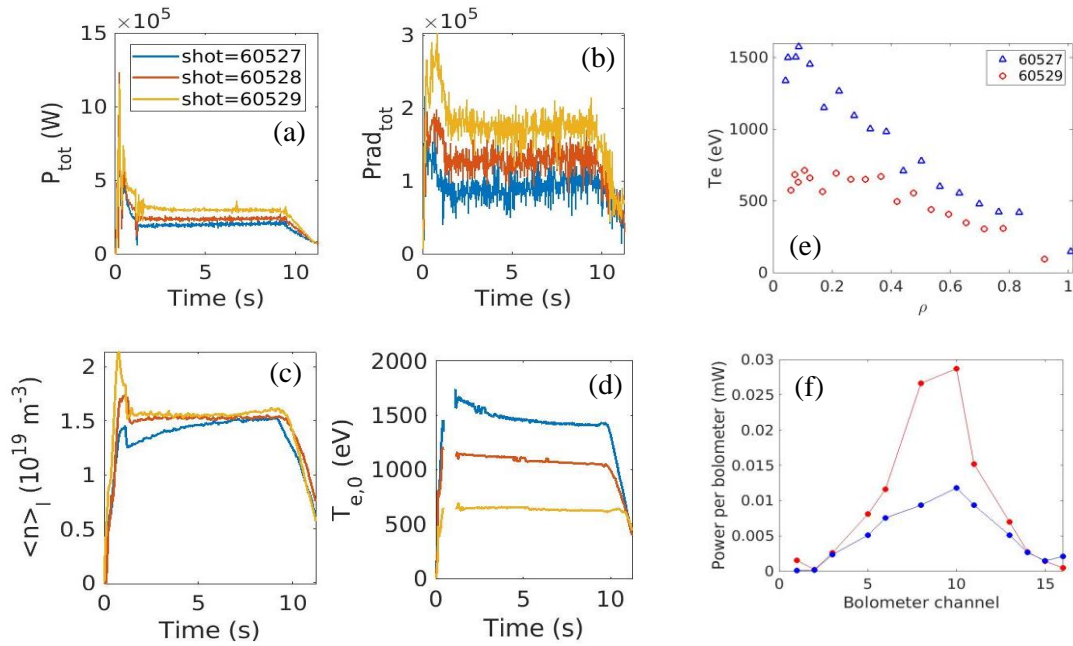


Figure 3: Time traces of ohmic power (a), total radiated power (b), line averaged density (c) and central electron temperatures (d) for 3 identically programmed consecutive pulses. Electron temperature profiles (e) and powers received by the 16 horizontal bolometry channels (f) are also shown.

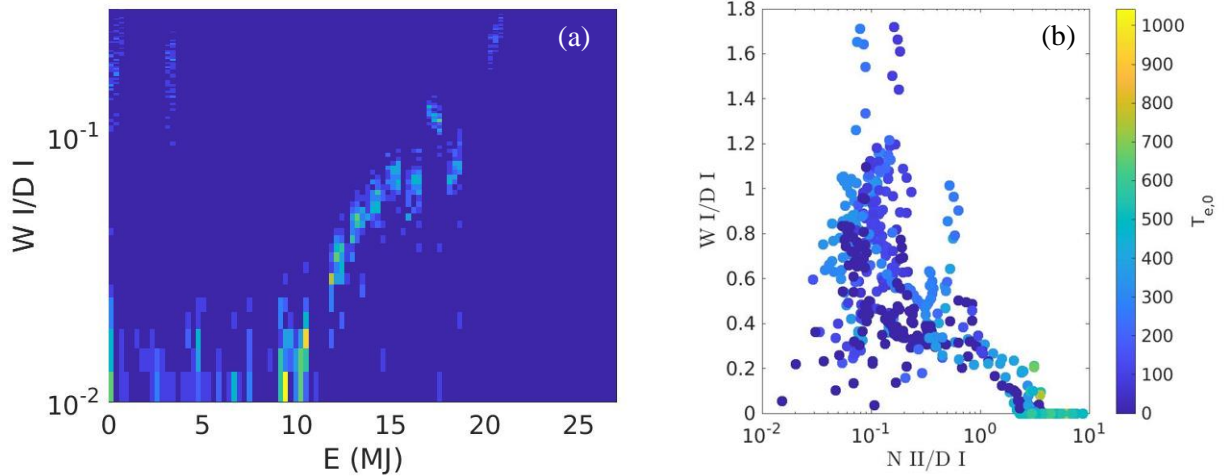


Figure 4: Impact of the distance to boronisation (a), in terms of energy injected during the limiter configuration, and nitrogen seeding (b) on the normalized neutral tungsten visible line intensity.

In the absence of available central heating to compensate core radiative cooling from tungsten, strategies were developed to minimize the negative impact of the limited phase on the rest of the pulse. The impact of boronisation is found to be lost relatively quickly with ~ 10 MJ of injected energy in this configuration which amounts to 20-30 pulses with ~ 1 s long inner limited phases. To cop with the quick loss of the impact of boronisations, nitrogen seeding was used, similarly to previous WEST campaigns [6], and was found to not only mitigate W sources but also increase the core confinement with larger central electron temperatures (Fig. 4). Together with fast X-point formations, reliable scenarios could be developed to avoid cold and MHD prone ohmic plasmas. Control of such scenarios in a larger range of plasma conditions remain to be developed.

Integrated modelling is performed with JINTRAC [7] up to the separatrix on the consecutive shots featuring changes in electron temperature profiles (Fig. 3). Turbulent transport is modeled with TGLF [8] and the neoclassical transport with NEO [9] for the main plasma species including

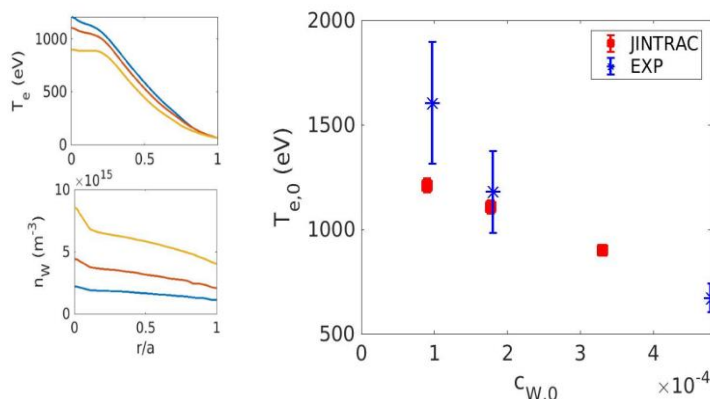


Figure 5: Temperature and tungsten profiles for increasing separatrix tungsten densities (left panels). Dependence of the central electron temperatures with the central tungsten concentrations from experimental

region and centrally peaked in the case where neoclassical thermal screening is reduced (Fig. 5). This provides estimate of the impact of the edge tungsten density consistently on core radiation and ohmic heating. Further modelling activities will benefit from physics informed boundary conditions for accurate descriptions of such nonlinearities.

In these WEST limiter experiments, two main aspects were investigated. First the startup without boronisation on pristine bulk tungsten tiles located on the inner limiters (HFS) has proven to be difficult due to low Z contamination of the plasma, uncontrolled densities and lack of external central heating. The need for boronisation is shown to be critical in these conditions to have a smooth plasma restart independently of the limiters material. Second, a range of plasma parameters (densities, plasma current, distance to boronisation, nitrogen seeding) was explored to provide an experimental basis on which validation of edge/core transport models can be performed in this phase where an equilibrium between core contamination and W sources is expected [11]. Frameworks, where both domains are consistently evolved with high fidelity models, are of particular interest for such analyses and extrapolations to future devices, e.g. [10]. Finally it has to be noted that different plasma conditions in limiter configurations were also explored on EAST and AUG as well [12].

References

- | | |
|--|---|
| [1] A. Loarte <i>et al</i> , <i>PPCF</i> 67 065023 (2025) | [7] M. Romanelli <i>et al</i> , <i>PFR</i> , 9 , 3403023 2014) |
| [2] D Fajardo <i>et al</i> <i>PPCF</i> 67 015020 (2025) | [8] G.M. Staebler <i>et al</i> , <i>NF</i> 61 116007 (2021) |
| [3] J. Bucalossi <i>et al</i> , <i>NF</i> 62 042007 (2022) | [9] E.A. Belli and J. Candy, <i>PPCF</i> 50 095010 (2008) |
| [4] C. Guillemaut <i>et al</i> , <i>NF</i> 65 036007 (2025) | [10] N. Varadarajan <i>et al</i> , <i>PFMC</i> (2025) |
| [5] R. Neu <i>et al</i> , <i>Phys. Scr.</i> 014038 (2009) | [11] R. Pitts <i>et al</i> , <i>NME</i> 42 101854 (2025) |
| [6] P. Maget <i>et al</i> , <i>PPCF</i> 64 045016 (2022) | [12] J. Hobirk <i>et al</i> , IAEA FEC (2025) |